JACS
JOURNAL OF THE AMERICAN CHEMICAL SOCIETY
pubs.acs.org/JACS
Article

Efficient Intermolecular Charge Transport in π-Stacked Pyridinium Dimers Using Cucurbit[8]uril Supramolecular Complexes

Hao Yu,[#] Jialing Li,[#] Songsong Li, Yun Liu, Nicholas E. Jackson, Jeffrey S. Moore, and Charles M. Schroeder*

Cite This: J. Am. Chem. Soc. 2022, 144, 3162−3173
Read Online
ACCESS | Metrics & More | Article Recommendations | Supporting Information

ABSTRACT: Intermolecular charge transport through π-conjugated molecules plays an essential role in biochemical redox processes and energy storage applications. In this work, we observe highly efficient intermolecular charge transport upon dimerization of pyridinium molecules in the cavity of a synthetic host (cucurbit[8]uril, CB[8]). Stable, homoternary complexes are formed between pyridinium molecules and CB[8] with high binding affinity, resulting in an offset stacked geometry of two pyridiniums inside the host cavity. The charge transport properties of free and dimerized pyridiniums are characterized using a scanning tunneling microscope-break junction (STM-BJ) technique. Our results show that π-stacked pyridinium dimers exhibit comparable molecular conductance to isolated, single pyridinium molecules, despite a longer transport pathway and a switch from intra- to intermolecular charge transport. Control experiments using a CB[8] homologue (cucurbit[7]uril, CB[7]) show that the synthetic host primarily serves to facilitate dimer formation and plays a minimal role on molecular conductance. Molecular modeling using density functional theory (DFT) reveals that pyridinium molecules are planarized upon dimerization inside the host cavity, which facilitates charge transport. In addition, the π-stacked pyridinium dimers possess large intermolecular LUMO−LUMO couplings, leading to enhanced intermolecular charge transport. Overall, this work demonstrates that supramolecular assembly can be used to control intermolecular charge transport in π-stacked molecules.

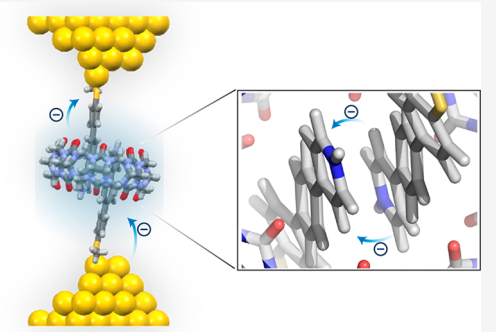

INTRODUCTION

Intermolecular charge transport in π-stacked aromatic groups is central to organic electronics[1] and biological processes.[2] In the field of organic electronics, it is widely believed that device efficiency critically depends on interchain charge transport between π-conjugated molecules.[3−5] In biology, charge transport through π-stacked DNA base pairs[6,7] and aromatic amino acid residues[6,7] plays a key role in metabolism,[8] photosynthesis,[9] and oxidative damage and repair of DNA.[10] From this view, understanding intermolecular charge transport through π-stacked molecules is essential for elucidating the fundamental mechanisms behind biological redox processes and for designing new materials for organic electronics.

Despite recent progress, it remains challenging to experimentally study intermolecular charge transport between aromatic groups at the molecular level. Prior work has provided evidence for through-space charge transport across a π-system by leveraging the structural character of [2,2]-paracyclophane.[11,12] However, challenges lie in building well-defined molecular geometries and controlling the spatial arrangements and orientations of aromatic rings to enable strong orbital coupling between adjacent molecules. In the field of single-molecule electronics, an alternative approach for studying intermolecular charge transport is to prepare π-conjugated molecules with only one terminal anchor group, which enables the formation of single-stacked molecular junctions by spontaneous π−π stacking. Prior work has used this strategy to show that intermolecular charge transport generally results in a 10-fold decrease in conductance compared to intramolecular transport in oligophenylene ethynylenes (OPEs) and fluorene molecular junctions.[13−16] Recent work has reported that intermolecular charge transport in π-stacked dimers is enhanced in imidazole-based junctions and is independent of conjugated structure length in thiophene-based junctions.[17,18] In addition, it was reported that electric fields induce the formation of terphenyl stacked dimers using single-molecule techniques.[19] However, different π-stacked geometries such as parallel offset or T-shape arrangements of aromatic rings are known to occur in experiments, which complicates the interpretation of experimental data and comparison to theoretical models.[20] For these

Received: December 3, 2021
Published: February 11, 2022

https://doi.org/10.1021/jacs.1c12741
J. Am. Chem. Soc. 2022, 144, 3162−3173

reasons, direct experimental measurement of charge transport in discrete aromatic dimers with well-defined geometries, separation distances, and stacking arrangements remains challenging.

Recently, supramolecular assembly has been used to build structures with well-defined geometries for molecular electronics.[21] For example, cucurbit[8]uril (CB[8]) and crown ether have been used to form [2]rotaxane structures to study the effect of host−guest interactions on intrachain charge transport.[22−24] Despite these advances, the application of supramolecular assembly to understand intermolecular charge transport has been far less explored. Discrete, π-stacked dimers with well-defined stacking geometries and separation distances provide an ideal model system to investigate intermolecular charge transport. To address this challenge, here we used the rigid synthetic macrocyclic host CB[8] to form defined ternary binding complexes (Scheme 1a). CB[8] exhibits unique molecular recognition characteristics enabling dimerization of specific guest molecules inside the cavity of CB[8] in a controlled manner.[25] Molecular complexation with CB[8] offers a facile approach to precisely position two aromatic groups in close proximity in a π-stacked orientation,[26] thereby enabling the investigation of intermolecular charge transport in discrete dimers.

Prior computational studies reported enhanced intermolecular charge transport between strongly interacting π-conjugated aromatic molecules with separation distances less than 4 Å.[27,28] Single crystal data and molecular modeling show that the stacking distance between the aromatic guest molecules in the cavity of CB[8] is generally around 3.6 Å.[29,30] We therefore conjectured that CB[8]-mediated dimerization of guest molecules would provide an ideal platform to investigate intermolecular charge transport using single molecule techniques.

Scheme 1. (a) Schematic of Molecular Design for Studying Intermolecular Charge Transport Using Synthetic Macrocycle-Mediated Dimerization; (b) Schematic of Molecular Junction Formed by a Single Pyridinium Molecule or Host−Guest Ternary Complex

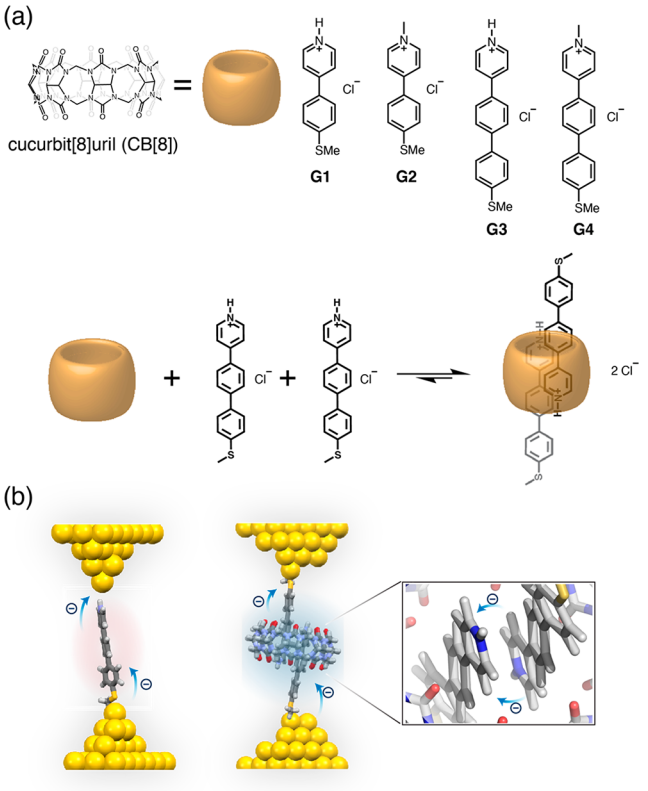

In this work, we study the charge transport properties of discrete pyridinium dimers stabilized by the synthetic host molecule CB[8] (Scheme 1b). As a functional motif, pyridinium is used in several applications including CO_2 reduction, organic light-emitting devices (OLEDs), and redox flow batteries.[31−33] From this view, understanding charge transport in pyridiniums is essential for designing new organic electronic materials. Herein, four pyridinium guest molecules (**G1−G4**) were used to investigate intra- and intermolecular charge transport using the CB[8]-mediated self-assembly approach. Molecular complexes were extensively characterized by NMR, X-ray diffraction (XRD), isothermal titration calorimetry (ITC), UV−vis absorption, fluorescence emission spectra, and density functional theory (DFT) simulations. Our results show that the pyridinium guests are dimerized into the cavity of CB[8] in a head-to-tail geometry with high binding affinity and compact π−π stacked structures. We directly measured the intermolecular conductance through pyridinium dimers using a scanning tunneling microscope-break junction (STM-BJ) technique. Remarkably, single-molecule conductance experiments show that intermolecular conductance through pyridinium dimers is comparable to the intramolecular conductive pathway. XRD crystal analysis and DFT simulations show that pyridinium molecules undergo planarization upon dimerization inside the host cavity, thereby facilitating efficient charge transport. Moreover, electronic coupling calculations show that the tight π-stacked geometry imposed by the host−guest interaction leads to strong intermolecular electronic coupling comparable to common organic semiconductors such as perylenediimide (PDI) and pentacene,[34,35] suggesting that efficient intermolecular charge transport is accessible. We further studied the role of the synthetic host on charge transport using a structural homologue of the host molecule, which revealed that the host molecule does not directly participate in charge transport. In addition, our results show that the counterion plays a key role in molecular conductance. Broadly, our work provides an improved understanding of intermolecular charge transport in well-defined π-stacked pyridiniums, suggesting that host−guest complexes provide a valuable set of modular molecular components for building π-stacked geometries for molecular electronic devices.

RESULTS AND DISCUSSION

Design, Synthesis, and Characterization of Complexes. We designed and synthesized four pyridinium derivatives (**G1−G4**) by protonating or methylating the corresponding arylpyridine (Supporting Information Figures S1−S6). To perform single-molecule conductance measurements, guest molecules were terminated with methyl sulfide (−SMe) which serves as an anchor group for making robust connections to gold electrodes.[36−38] In this way, a discrete molecular junction is formed that promotes through-space charge transport between π-stacked pyridinium dimers, as shown in Scheme 1b. The donor−acceptor character of monocationic 4-phenylpyridinium molecules, together with the close spatial proximity imposed upon binding in a head-to-tail

https://doi.org/10.1021/jacs.1c12741
J. Am. Chem. Soc. 2022, 144, 3162−3173

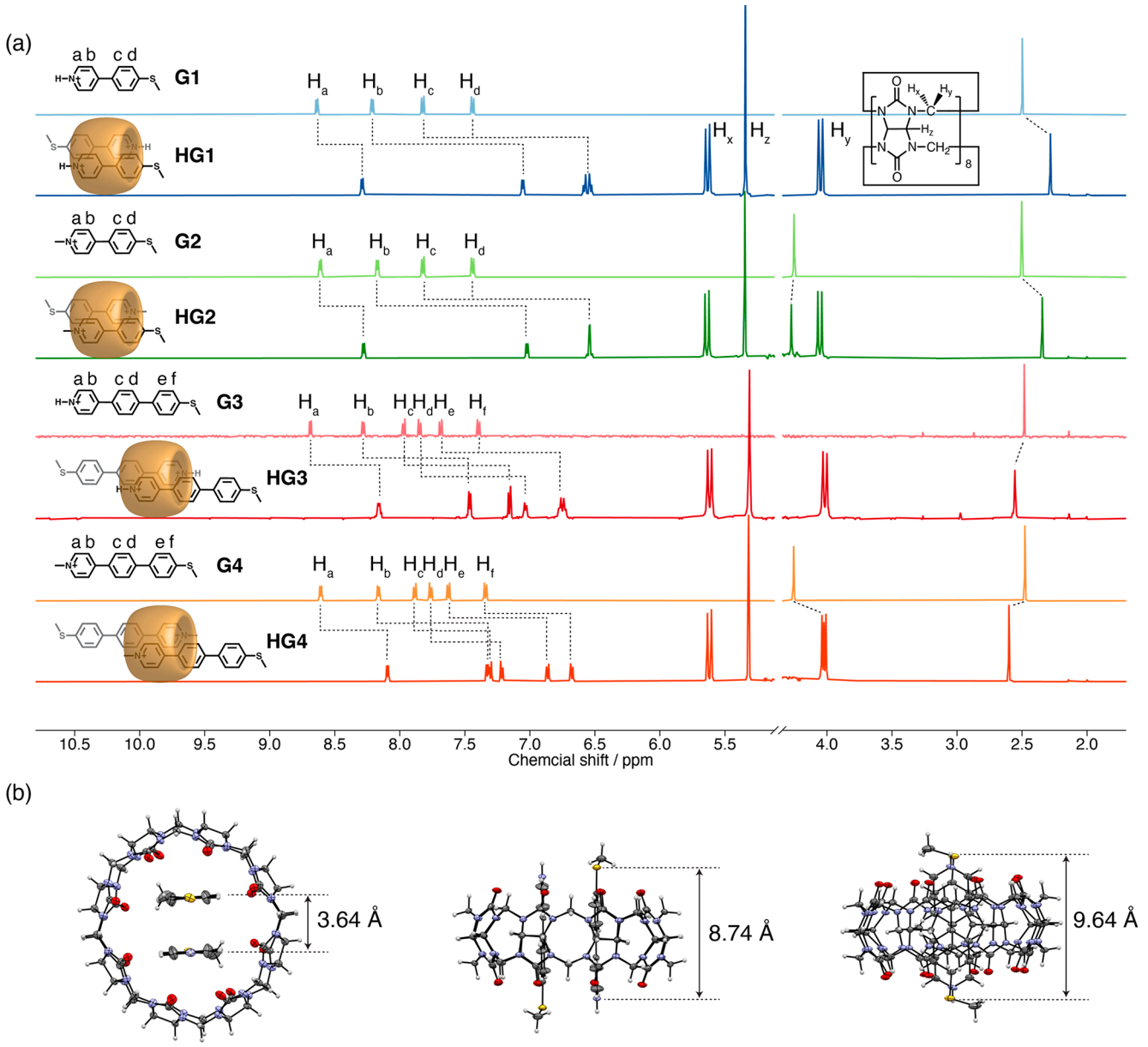

Figure 1. Chemical characterization of host–guest complexes. (a) ^{1}H NMR spectra (500 MHz, D_2O, 0.5 mM, 298 K) of the ternary complexes (**HG1**–**HG4**) and corresponding guest molecules (**G1**–**G4**). The host–guest molar ratio in the complex is 1:2. Counterions (Cl^-) and NMR signals between δ 5.0 and 4.5 ppm have been omitted for clarity. Protonated pyridiniums were prepared *in situ* by mixing corresponding pyridine with 27 equiv of DCl. (b) Crystal structure of **HG1**. Distances are shown to define the geometry of homoternary complexes.

geometry in CB[8] cavities, leads to strong π–π coupling in pyridinium dimers known as aromatic donor–acceptor interaction.[29,39–41]

Following synthesis, complexation between pyridinium and CB[8] was characterized using ^{1}H NMR. Upon addition of 0.5 equiv of CB[8] to a solution of **G1**–**G4**, the proton signals of guest molecules show a marked shift (Figure 1a), indicating the formation of a 2:1 homoternary complex. Each proton was assigned based on 2D ^{1}H–^{1}H correlation spectroscopy (COSY) NMR spectra (Figures S7–S10). It is known that the proton signals of guest molecules shift to higher fields upon dimerization into the cavity of CB[8], whereas the resonances of protons outside the cavity exhibit a downfield shift.[42,43] All proton resonances residing on aromatics display large upfield shifts ($\Delta\delta$ > 0.5 ppm) upon binding, indicating that the aromatic moiety resides inside the cavity of CB[8]. Moreover, the methyl sulfide resonance in **G1** and **G2** exhibits a slight upfield chemical shift of ca. 0.2 ppm, suggesting that these moieties are slightly encapsulated by CB[8], while the methyl sulfide proton signal in **G3** and **G4** slightly shifts to lower fields, confirming that the SMe group in these molecules is located outside the CB[8] cavity. The binding geometries inferred from NMR are summarized in Figure 1a.

The formation of a discrete 2:1 homoternary complex was further confirmed by ^{1}H NMR titrations (Figures S11–S14) and 2D rotating-frame nuclear Overhauser effect (ROESY) and diffusion ordered NMR spectroscopy (DOSY) (Figures S15–S27). Notably, both free and bound guest molecules **G1**–**G4** exhibit distinct and sharp NMR signals in titration experiments, indicating that the association and dissociation of host–guest complexes undergo slow exchange equilibrium on the NMR time scale. Furthermore, DOSY experiments show

https://doi.org/10.1021/jacs.1c12741
J. Am. Chem. Soc. 2022, 144, 3162–3173

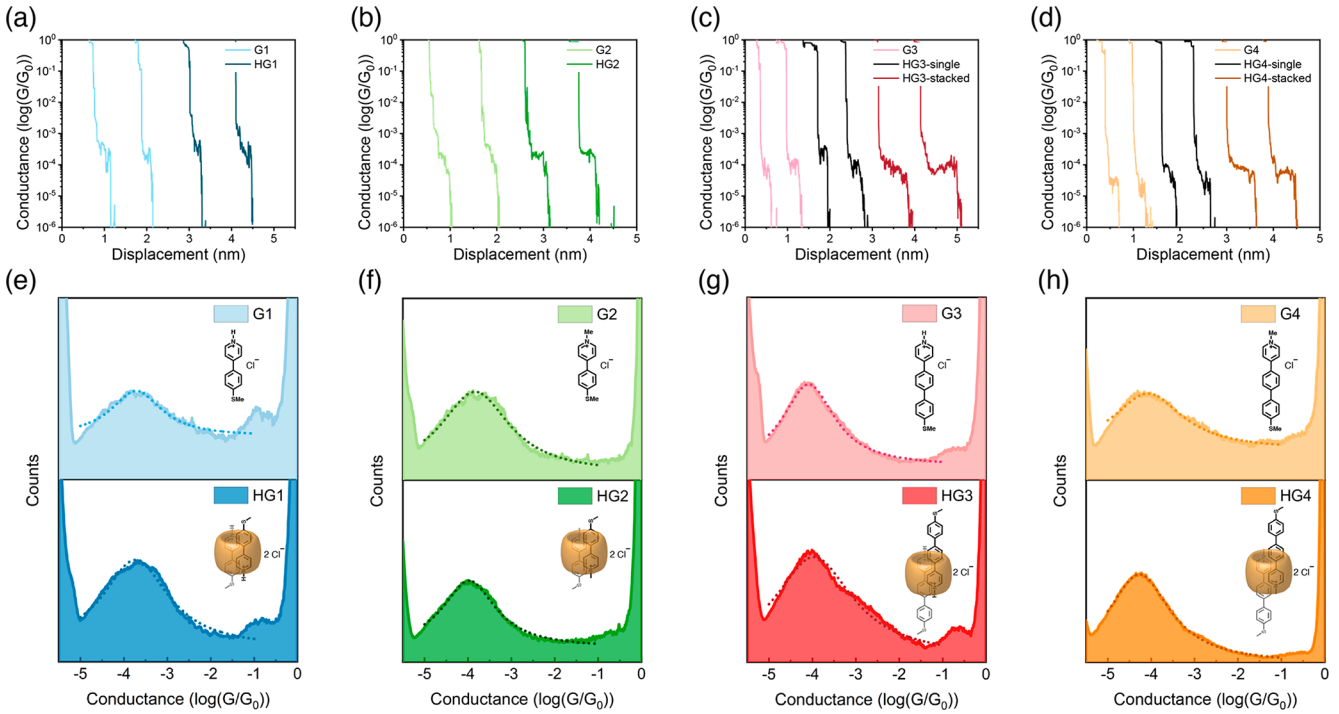

Figure 2. Single molecule conductance of host–guest molecules. (a-d) Characteristic single molecule conductance traces for **G1**–**G4** and **HG1**–**HG4** (applied bias 0.25 V). STM-BJ experiments were performed using 0.5 mM aqueous solution (in 50 mM sodium acetate buffer, pH = 4.8). All host–guest complexes **HG1**–**HG4** have chloride counterions. For the ternary complexes **HG3** and **HG4**, two different types of single molecule conductance traces are observed corresponding to junctions formed by unbound pyridinium and the ternary complex. For **HG1** and **HG2**, the two different conductance pathways are generally not distinguishable in our measurements. Here, $G_0 = 77.5\ \mu S$ is the quantum unit of conductance. (e-h) Series of 1D conductance histograms for guest molecule (top) and corresponding binding complex (bottom) (applied bias 0.25 V). Dotted lines show Lorentzian fits.

that the diffusion coefficient (D) of the unbound guest (**G1**–**G4**) in aqueous solution is in the range $(5.3–6.5) \times 10^{-10}$ m^2/s. Smaller values of D were observed for the homoternary complexes ranging in the range $(2.6–2.7) \times 10^{-10}$ m^2/s, which are generally less than that of free CB[8] ($D = 3.1 \times 10^{-10}$ m^2/s) (Table S1).[44] These results support the formation of a single, well-defined complex involving the stacking of two pyridinium guest molecules held together by a CB[8] host. In addition, the binding complexes **HG1**–**HG4** exhibit bathochromic shifts in UV–vis absorption and fluorescence emission maxima, suggesting that π–π stacking in pyridinium dimers results in electron-delocalization in guest molecules (Figure S28).[29,44]

Geometrical parameters of the homoternary complex were determined using XRD analysis of a single crystal of **HG1** (Figure 1b, Supporting Information Section S5). Crystal structure analysis clearly shows that two independent molecules of **G1** are encapsulated in the cavity of CB[8] in a head-to-tail offset stacking with a distance of 3.64 Å, a typical distance for aromatic stacking.[41] In addition, binding constants (K_a) for the formation of ternary complex and related thermodynamic parameters were determined from ITC and NMR (Supporting Information, Section S6, Figures S29–S30, and Table S3). The large K_a value (>10^7 M^{-2}) indicates a strong binding affinity.[29,40] In addition, we assessed the ability to form a 1:1:1 heteroternary complex by mixing two different guest molecules with equimolar amounts of CB[8]. However, NMR results revealed a mixture of various binding complexes rather than a single well-defined complex (Figures S31–S32).

Single-Molecule Conductance of Pyridinium Dimers. We used the scanning tunneling microscope-break junction (STM-BJ) technique to characterize the charge transport properties of guest molecules and host–guest complexes. In all cases, STM-BJ measurements were performed in aqueous solution at identical concentrations as NMR experiments, and the results from 10^3 to 10^4 individual measurements were compiled into histograms for statistical analysis (Supporting Information, Section 1).[42,43] A single STM-BJ measurement is generally completed in 250–350 ms with a tip pulling rate of 20 nm/s, thereby requiring approximately 2–3 h for data collection of a large molecular ensemble for robust statistical analysis. NMR experiments suggest that the complexation undergoes slow exchange equilibrium longer than the second time scale (Scheme 1a). Based on the characteristic time scale for complex disassociation, the host–guest complex is expected to remain associated and bound over the time scale of the STM-BJ experimental measurement, which enables linkage to the gold electrode. In general, we observed both the bound (stacked pyridinium dimer) and unbound (free pyridinium) state of the host–guest complexes at equilibrium in STM-BJ experiments. Complexes **HG1**–**HG4** contain two anchor groups (–SMe) from the two encapsulated guest molecules, thereby enabling linkage to gold electrodes and the formation of robust molecular junctions.[38] On the other hand, positively charged pyridinium groups can link to gold electrodes via electrostatic interactions.[47,48] Therefore, guest molecules not bound in host–guest complexes form molecular junctions coupled through the terminal SMe and pyridinium groups (Scheme 1b).

Characteristic single-molecule conductance-displacement traces for **G1**–**G4** and **HG1**–**HG4** are shown in Figure 2a–d. Detailed analysis on individual molecular conductance traces

https://doi.org/10.1021/jacs.1c12741
J. Am. Chem. Soc. 2022, 144, 3162–3173

for **HG3**−**HG4** solutions show two distinct behaviors. The dominant conductance traces exhibit larger electrode-electrode displacement which can be assigned to the fully formed homoternary complex, whereas a small fraction of conductance traces is assigned to the free guest molecule by direct comparison with the conductance traces of the corresponding free guest molecules. These results are consistent with chemical characterization which indicates that the formation of bound complexes is highly favorable. In general, the stacked pyridinium dimer of **HG1**−**HG4** exhibits a comparable molecular conductance ($\sim 10^{-3}$−10^{-4} G_0) to the corresponding unbound pyridinium (**G1**−**G4**). Prior work using single-molecule force spectroscopy (SMFS) suggested that the binding force of a CB[8] ternary complex is around 0.14−0.16 nN,[49] which is similar in magnitude to the strength of Au-SMe interactions measured by conductive AFM (0.5 nN).[50] In our measurements, the conductance-displacement traces show that the junction displacements at breakage are consistent with fully formed host−guest complexes, suggesting that the binding complexes generally remain intact until junction breakage.

Individual molecular conductance traces are compiled into one-dimensional (1D) histograms without data selection (Figure 2e−h), which enables determination of the maximum average molecular conductance by fitting to a Lorentzian function.[51] Our results show that the stacked pyridinium dimers in **HG1**−**HG4** have a conductance plateau around 10^{-4} G_0, which is comparable to free pyridinium molecules (**G1**−**G4**). We further analyzed the results from **HG3** solutions to determine possible shoulders or obscured peaks using the holding mode of operation of STM-BJ (Figures S33 and S34), wherein **HG3** molecular junctions are held at a fixed position for 150 ms and transient molecular conductance is measured. Our results show that the molecular conductance of **HG3** solutions is well described by a primary conductance peak around $\sim 10^{-3.7}$ G_0. The possible shoulder around 10^{-3} G_0 is attributed to geometry changes or junction rupture during the pulling process in the tapping mode of operation of STM-BJ. In general, we did not observe evidence of stable dimer junction formation for free guest molecules in the absence of host.

To further understand the charge transport behavior of host−guest complexes, two-dimensional (2D) histograms of conductance versus displacement and molecular displacement distribution histograms were used to analyze **G1**−**G4** and **HG1**−**HG4** (Figures 3a−d and S35−S40). Prior STM-BJ measurements have shown that the displacement between electrodes is directly correlated with the contour length of the molecule held in the junction.[52,53] Our results show that the conductive pathways of **G1** and **G2** exhibit a relative tip-to-substrate displacement of ∼0.2 nm, which is close to that of **HG1** and **HG2** (Figures S35−S36). Crystal structures show that the end-to-end molecular lengths of pyridinium dimers in **HG1** and **HG2** are approximately the same as those for the corresponding single pyridinium molecules. However, the 2D conductance histograms for **G3** and **G4** show that the molecular conductance is associated with a small relative tip-to-substrate displacement of ∼0.2−0.3 nm (Figure 3a−b), whereas charge transport in the pyridinium dimers in **HG3** and **HG4** occurs with larger molecular extensions of ∼0.6−0.7 nm (Figure 3c−d). In general, the increase in molecular length for **HG3** and **HG4** is consistent with the structures of the supramolecular complexes interpreted from NMR characterization. We further performed a series of control experiments to assess the molecular conductance of the synthetic host molecule CB[8] in the absence of guest molecules. Our results show no significant molecular conductance in the range 10^{-5}−10^{0} G_0 for CB[8] alone (Figure S37), which suggests that the host molecule does not directly contribute to the molecular conductance features in solutions of **HG1**−**HG4** complexes.

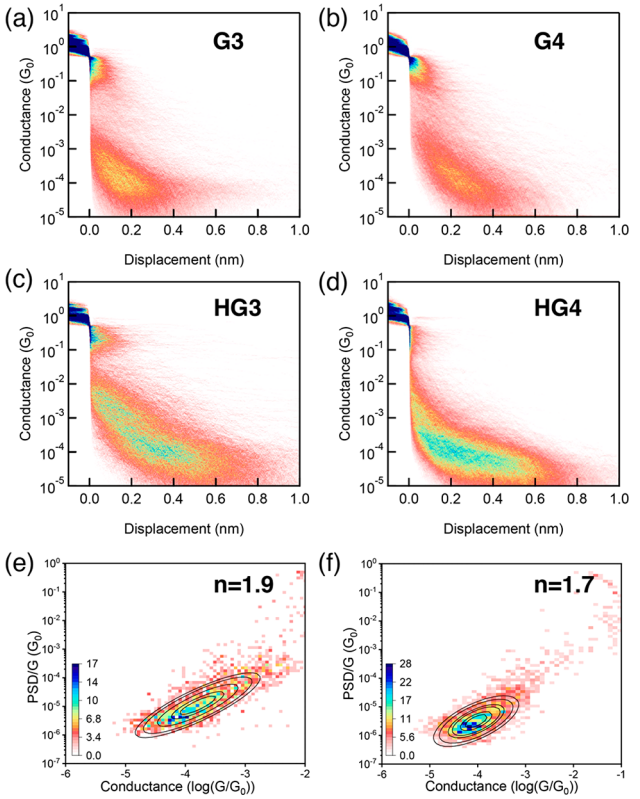

Figure 3. 2D conductance histograms (applied bias 0.25 V) of **G3** (a), **G4** (b), **HG3** (c), and **HG4** (d). 2D histograms of noise power/G as a function of average conductance for (e) **HG3** and (f) **HG4**, respectively. Scaling exponents (n) are determined by normalizing noise power by G^n until the bivariate normal distribution gives a correlation of approximately zero between normalized noise power and average conductance.

To further investigate intermolecular charge transport in pyridinium dimers, we used flicker noise analysis (Figures 3e−f and Figures S41−S44). For these experiments, molecular junctions are captured and held at a fixed position for ∼150 ms while conductance fluctuations are determined. Traces that contain junctions within 1.5 standard deviations of the average conductance values are selected, and noise is quantified by numerically integrating the conductance noise power spectral density (PSD) between frequencies of 100 and 1000 Hz.[54] Prior work by Venkataraman and co-workers[16,17] and Hong and co-workers[18,19] has shown that intermolecular charge transport results in large variations in noise and average conductance, and the correlation is quantified by the scaling exponent (n) of the normalized noise power (noise power/G^n) versus the average normalized conductance (G). A scaling exponent of $n \approx 2$ suggests through-space transmission in the coupled molecular junction, whereas an exponent $n \approx 1$ corresponds to through-bond transport. Our results clearly show that molecular conductance in **HG3** (n = 1.9) and **HG4** (n = 1.7) complexes occurs by through-space transmission. These results further support the notion that charge transport

https://doi.org/10.1021/jacs.1c12741
J. Am. Chem. Soc. 2022, 144, 3162−3173

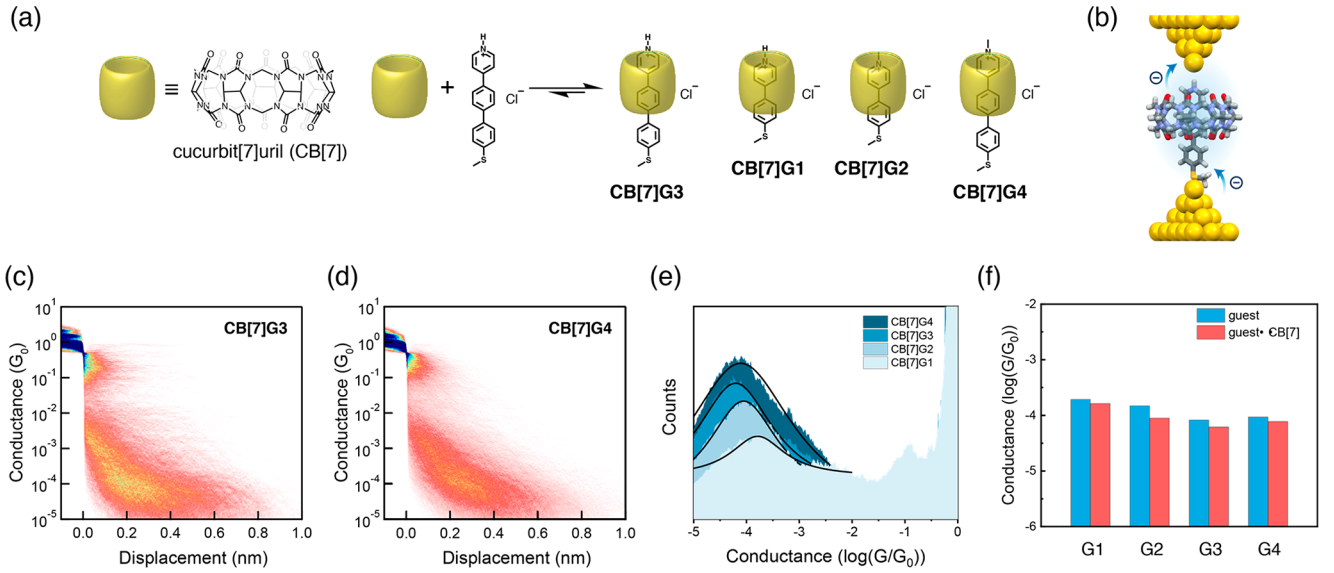

Figure 4. Understanding the role of the synthetic host on charge transport. (a) Chemical structure of CB[7] and binding equilibrium between CB[7] and pyridinium. (b) Schematic illustration of single molecule break junction formed by CB[7]-mediated binary complex. (c-d) 2D conductance histograms of binary complexes **CB[7]G3** and **CB[7]G4**. (e) 1D conductance histograms of CB[7]-mediated binary binding complexes. Molecular conductance is determined by Lorentzian fitting ranging from 10^{-2} to 10^{-5} G_0 (solid line). (f) Comparison of the conductance of free pyridiniums and CB[7]-bound pyridiniums.

in host−guest complexes involves coupled intermolecular charge transport in pyridinium dimers.

Attempts at measuring the conductance noise PSD of guest molecules **G1**−**G4** alone were unsuccessful, likely due to the weak coupling interactions between pyridiniums and gold electrodes, which decreased junction stability during the holding mode of operation of STM-BJ. These observations further support the notion that two terminal SMe groups allow for stable junction formation for stacked pyridinium dimers in host−guest complexes **HG1**−**HG4**. Overall, the PSD analysis suggests that charge transport in the ternary complexes occurs through a through-space transmission within the capsulated dimer.

Charge transport in guest molecules **G1**−**G4** occurs via an intramolecular pathway, whereas charge transport in host−guest complexes **HG1**−**HG4** occurs by through-space coupling or intermolecular transport between adjacent stacked pyridinium dimers in the host cavity. Prior work reported that intermolecular charge transport in single-stacked terphenyl, oligophenylene ethynylene, or fluorene junctions generally results in a 10-fold *decrease* in molecular conductance compared to the intramolecular pathway,[13−16,19] which is fundamentally different than our observations for stacked pyridiniums in host−guest complexes (Figures 2 and 3). From this view, it is remarkable that **HG1**−**HG4** complexes show comparable single-molecule conductance with their corresponding guest molecules, despite the qualitatively different charge transport pathways for supramolecular complexes. Based on these results, we aimed to understand the underlying charge transport mechanism using a series of control experiments and DFT simulations.

Analysis of Intermolecular Charge Transport. Charge transport in molecular junctions is generally affected by molecule−electrode contacts.[38,55] In our experiments, host−guest complexes **HG1**−**HG4** are linked to electrodes via symmetric Au−S interactions. However, guest molecules **G1**−**G4** are linked to electrodes by asymmetric interactions consisting of a Au−S bond at one terminus and a weaker electrostatic interaction between pyridinium and the Au electrode at the other terminus. Prior work has shown that weaker coupling in anchor−electrode contacts and asymmetric contacts decrease molecular conductance.[56−58] To understand the nature of electrode contact interactions and the impact on molecular conductance in guest molecules, we performed a series of control experiments using two arylpyridine molecules (**PY1** and **PY2**, Figures S45 and S46). Our results show that pyridinium guest molecules **G1**−**G4** exhibit slightly lower conductance values compared to the corresponding arylpyridine molecules, which is attributed to weaker coupling between the electrode and pyridinium compared to pyridine. Notably, **PY2** exhibits similar molecular conductance compared to the stacked pyridinium dimers (around 10^{-4} G_0), despite the fact that the charge transport in arylpyridine is dominated by intramolecular transmission through a shorter end-to-end molecular length compared to the binding complexes (Figure S47). Furthermore, a terphenyl molecule with symmetric −SMe contacts was reported to show an intramolecular conductance around $10^{-3.5}$ G_0, and the corresponding stacked dimer shows molecular conductance around 10^{-5} G_0,[19] which is smaller than the average molecular conductance of π-stacked pyridinium dimers measured in this work. These results indicate that symmetric contacts alone in the ternary complexes are not sufficient to explain the unexpectedly large conductance for π-stacked pyridinium dimers in our experiments.

We further sought to understand the role of the synthetic host CB[8] on the charge transport properties of pyridinium dimers. Prior work by Niu and co-workers reported that bipyridinium (viologen) shows enhanced molecular conductance when threaded into a CB[8] cavity in a 1:1 binding complex due to reduced outer sphere reorganization energy.[22] However, this conclusion was challenged in a subsequent publication in which the formation of 2:2 quaternary complexes between arylviologen and CB[8] was reported.[59]

https://doi.org/10.1021/jacs.1c12741
J. Am. Chem. Soc. 2022, 144, 3162−3173

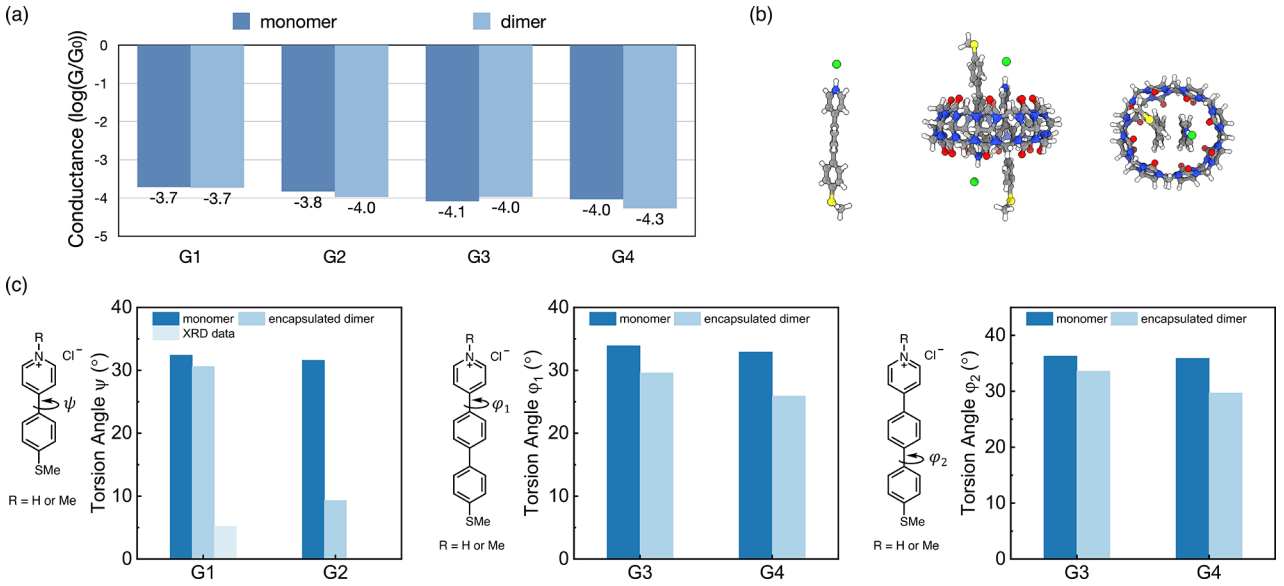

Figure 5. (a) Comparison of the molecular conductance between pyridinium monomers and encapsulated dimers **G1**, **G2**, **G3**, and **G4** (counterion: Cl^-). (b) Ball-and-stick representation of the optimized free pyridinium (**G3**) and ternary complex structure (**HG3**) at the wB97XD/6-31G(d,p) level of theory using SMD solvation model for water. Counterion (Cl^-) is shown in green. (c) Comparison of average torsion angle between free and encapsulated pyridinium molecules.

To understand how the synthetic host affects the charge transport properties of stacked pyridinium, we use cucurbit[7]-uril (CB[7]), a smaller homologue to CB[8] (Figure 4a–b). CB[7] shows similar binding properties to CB[8] albeit with a smaller portal diameter (5.4 Å) compared to CB[8] (6.9 Å), which allows for the complexation of only one aromatic guest molecule (Figures S48–S55).[25,43] Results from STM-BJ experiments on host–guest complexes formed by CB[7] are shown in Figures 4c–e and S56. Comparisons between CB[7]-mediated binary complexes and free pyridiniums imply that changes in microenvironment upon encapsulation do not lead to an enhanced conductance (Figure 4f).

We further investigated the effect of counterions on the charge transport behavior of pyridinium dimers (Figure 5a, Supporting Information Section S9). Here, we changed the counterions of **HG2** and **HG4** to iodide (**HG2-I** and **HG4-I**) (Figures S57–S65) and added 1 mol equiv of iodide ions to solutions of **HG1** and **HG3**. We then performed the single-molecule conductance measurements and flicker noise analysis using the same setup and conditions. Our results show that the molecular conductance increases in the presence of iodide (Figures S66–S70). Iodide ions are known to interact with metallic electrodes and affect the electrode work function,[60–62] which suggests that these observations are due to the adsorption of iodide on gold electrode surfaces which changes the alignment between frontier molecular orbital energies of pyridinium molecules and the Fermi level of the gold electrode.

DFT Modeling and Simulations. We performed DFT simulations to understand the geometry of the π-stacked pyridinium dimer. Molecular modeling of **HG1** and **HG2** was performed using corresponding crystal data,[29] whereas DFT simulations of **HG3** and **HG4** were performed using a modified structure based on the crystal structure of a ternary complex formed by 4,4′-bipyridin-1-ium and CB[8].[30] In all cases, molecular geometries were optimized by Gaussian'16 using a range-separated functional (wB97XD) with a 6-31G(d,p) basis set and the SMD solvation model for water.[63] The wB97XD functional provides accurate geometries and energetics for systems containing noncovalent interactions including π–π interactions, as opposed to traditional functionals such as B3LYP.[64–66] Simulation results show that pyridiniums are dimerized into the cavity of CB[8] in a head-to-tail orientation with a compact π–π stacked geometry and longer sulfur–sulfur distance compared to free pyridinium molecules (Figures 5b and S71–S76), which is in good agreement with NMR results. Notably, DFT simulations suggest that the average interplane torsional angle of the pyridinium molecules decreases upon dimerization inside the cavity of the host (Figure 5c). These results are consistent with XRD crystal data for **HG1** and **HG2**, which indicate that pyridinium molecules have a planar geometry with a torsion angle below 10° (Figure 1b). Prior work reported that the molecular conductance of π-conjugated structures increases with a decreased interplanar torsion angle.[51,67,68] Taken together, these results suggest that the planarization imposed by the host–guest interaction facilitates efficient charge transport across the pyridinium dimer.

To further understand the charge transport properties in pyridinium dimers, we performed molecular modeling using nonequilibrium Green's function-density functional theory (NEGF-DFT) via the Atomistix Toolkit (ATK) package.[69,70] Pyridinium dimers including counterions were modeled using the DFT-optimized molecular geometry of the binding complex (wB97XD/6-31G(d,p) and SMD solvation model for water), and CB[8] was removed to lower the computational expense (simulation details are included in Supporting Information, Section S1 and Figures S77–82). The gold electrode was modeled using Au pyramids on a Au face-centered cubic (fcc) slab with periodic boundary conditions.[37,71] NEGF-DFT simulation results show resonances located relatively close to E_F. In particular, transmission spectra exhibit strong resonances above E_F. It is worth noting that a similar transmission function shape (i.e., an antiresonance transmission dip and two nearby resonance transmission peaks) was observed in conductance measurements of charge

https://doi.org/10.1021/jacs.1c12741
J. Am. Chem. Soc. 2022, 144, 3162–3173

transfer (CT) complexes formed by π-conjugated oligothiophene and tetracyanoethlene.[72,73] In these systems, the transmission function character was attributed to the Fano resonance which accounts for a 100-fold increase in molecular conductance. However, we did not observe evidence of charge transfer (e.g., CT band in UV/vis spectra) between the electron-rich thioanisole and the electron-deficient pyridinium of the guest in this work.

To understand the relationship between stacked geometries and charge transport, we used DFT to compute the electronic coupling integrals (V) between pyridiniums within the dimer complexes (Table 1). Dimer geometries are extracted from the

Table 1. Comparison of Intermolecular LUMO−LUMO Coupling of π-Stacked Pyridinium Dimers with and without Host Molecules

#	V_L (eV) with counterion	V_L (eV) without counterion	#	V_L (eV) with counterion	V_L (eV) without counterion
HG1	0.09	0.19	**G1 dimer**	0.04	0.16
HG2	0.12	0.15	**G2 dimer**	0.0009	0.07
HG3	0.09	0.20	**G3 dimer**	0.03	0.15
HG4	0.14	0.20	**G4 dimer**	0.15	0.18

optimization simulations of the full complexes, and the host complexes are not included. NEGF-DFT simulations suggest that conductance through the LUMO channel is favorable, so we determined the LUMO−LUMO coupling integral (V_L). V_L was computed at the wB97XD/6-31G(d,p) level of theory using a dimer projection (DIPRO) method.[74] V_L was computed in both the presence and absence of the chloride counterion. Our results show large coupling values (>0.1 eV) of the charge transport integrals similar to those predicted for high-mobility charge transport organic materials including perylenediimide whose V_L is around 0.1 eV.[1,35,75,76] Prior work on π-conjugated organic materials has shown that the electronic couplings decay by as much as a factor of ∼4 upon increasing the intercentroid distance from 3.4 to 4 Å.[1] In our system, DFT simulations and XRD analysis reveal that the intercentroid distance between π-stacked aromatic rings can be decreased to 3.4 Å (**HG2**) due to stabilization of the host molecule. Although the precise values of V_L will be sensitive to the local translation of the dimers, the values of V_L are significantly larger than thermal energy k_BT, which is consistent with large couplings at short intermolecular dimer distances. These results highlight the importance of tight $\pi-\pi$ coupling imposed by host−guest interactions in intermolecular charge transport.

As a control, we further used DFT to model spontaneous dimerization of pyridiniums in the absence of host molecules, and we compared the interplane torsional angle and electronic coupling integral with corresponding encapsulated pyridinium dimers (Table 1 and Figures S83−S89). Simulations were performed in the absence of the host compound using the wB97XD/6-31G(d,p)/SMD model (water). Our results show that the encapsulated dimers generally exhibit a smaller interplane torsional angle and a larger electronic coupling, suggesting that intermolecular charge transport in the encapsulated dimers is more energetically favorable. These results further support our interpretation that host−guest complexation facilitates intermolecular charge transport by creating tighter $\pi-\pi$ stacked geometries relative even to those formed by spontaneous dimerization.

Prior work on single-molecule junctions reported that extended conjugation patterns and significantly overlapped π-clouds enable efficient through-space charge transport, thereby leading to larger conductance values in the through-space transport pathway.[18,77,78] Our results further support the notion that electronic coupling at the stacking interface critically determines intermolecular charge transport in single-molecule junctions. In the present work, we find that the closely π-stacked pyridinium dimers exhibit similar molecular conductance close to free pyridinium monomers, whereas prior work generally reported a 10-fold *decrease* in the intermolecular pathway compared to the intramolecular pathway.[13−16,19] Overall, we attribute the unexpectedly large molecular conductance of the host−guest complexes to reduced interplanar torsion angles of the guest molecules upon encapsulation in the guest molecules, which leads to enhanced intramolecular charge transport. Moreover, tight $\pi-\pi$ stacked geometries stabilized by host−guest interactions enable strong intermolecular electronic coupling, and consequently lead to efficient intermolecular charge transport.

Finally, we further explored the structure−property correlations of host−guest complexes by expanding the scope of guest molecules (Supporting Information, Section S11). In particular, we identified a bipyridinium derivative that dimerizes inside the cavity of CB[8] with the electron-rich thioanisole inside the host, and the molecular junction is linked by the two pyridinium groups outside the cavity of CB[8]. Our results show that this complex exhibits a molecular conductance of $\sim 10^{-4}$ G_0, which is consistent with our results on **HG1**−**HG4**. Overall, these results showcase that the approach presented in this work are applicable beyond the structures described here.

CONCLUSIONS

In this work, we utilize self-assembly to achieve discrete and well-defined supramolecular molecular junctions, thereby enabling the study of intermolecular charge transport in π-stacked dimers. Whereas prior work has largely focused on understanding intramolecular charge transport in single π-conjugated junctions, our results show that the molecular conductance of pyridinium dimers is unexpectedly large upon dimerization and π-stacking in the cavity of CB[8]. Extensive chemical and physical characterization of the host−guest complexes shows that the pyridinium dimer stacks in a parallel offset arrangement with a longer end-to-end charge transport pathway. Results from DFT simulations together with experiments using structural analogues reveal that the efficient molecular conductance arises from the reduced torsion angle in the pyridinium molecule and the strong $\pi-\pi$ coupling in the pyridinium dimer, and the synthetic host CB[8] does not significantly affect the charge transport properties. Broadly speaking, this study offers a model system to investigate the charge transport properties of stable π-stacked dimeric structures. Moreover, the dynamic nature of host−guest complexes are promising designs of molecular electronic devices with stimuli-responsive properties.

Beyond the applications explored in this work, it is instructive to consider the potential limitations of using host−guest complexes for studying molecular charge transport. In this approach, guest molecules need to be carefully chosen

https://doi.org/10.1021/jacs.1c12741
J. Am. Chem. Soc. 2022, 144, 3162−3173

to enable (1) the formation of stable homoternary complexes, (2) head-to-tail stacking geometries in the cavity of CB[8], and (3) robust linkages to the metallic electrode for conductance measurements. Moreover, characterizing and analyzing molecular conductance in heteroternary complexes formed by CB[8] with two complementary guests is challenging. Prior work by Kiguchi and co-workers on $\pi-\pi$ stacked heterocomplexes revealed technical challenges in controlling molecular orientation in conductance measurements.[79] Nevertheless, our results suggest that the CB[8]-based host−guest chemistry offers promising opportunities to explore intermolecular charge transport between diverse aromatic groups. For example, selected radical cations including viologen[80] and tetrathiafulvalene[81] and amino acids such as phenylalanine[82] and tryptophan[83] dimerize inside CB[8], thereby providing a model system to understand the charge transport mechanism in redox-active materials and biological nanowires at the molecular scale.[21,84] Moreover, CB[8]-based dynamic complexes have been used to build supramolecular switches that reversibly transform by the application of external stimuli such as light, redox potential, or pH.[85] In this way, merging the unique host−guest chemistry and single-molecule conductance experiments will provide new approaches for functional molecular electronics.

■ ASSOCIATED CONTENT

Supporting Information

(PDF) (CIF) The Supporting Information is available free of charge at https://pubs.acs.org/doi/10.1021/jacs.1c12741.

> Description of chemical synthesis of pyridinium molecules, chemical and physical characterization of host−guest binding complexes, experimental details on STM-BJ, simulation methods, supporting text, and supporting figures; crystal data for **HG1** (PDF)

Accession Codes

CCDC 2069475 contains the supplementary crystallographic data for this paper. These data can be obtained free of charge via www.ccdc.cam.ac.uk/data_request/cif, or by emailing data_request@ccdc.cam.ac.uk, or by contacting The Cambridge Crystallographic Data Centre, 12 Union Road, Cambridge CB2 1EZ, UK; fax: +44 1223 336033.

■ AUTHOR INFORMATION

Corresponding Author

Charles M. Schroeder − *Department of Chemical and Biomolecular Engineering, Department of Materials Science and Engineering, Department of Chemistry, and Beckman Institute for Advanced Science and Technology, University of Illinois at Urbana−Champaign, Urbana, Illinois 61801, United States; Joint Center for Energy Storage Research, Argonne National Laboratory, Lemont, Illinois 60439, United States;* orcid.org/0000-0001-6023-2274; Email: cms@illinois.edu

Authors

Hao Yu − *Department of Chemical and Biomolecular Engineering, University of Illinois at Urbana−Champaign, Urbana, Illinois 61801, United States;* orcid.org/0000-0002-1594-769X

Jialing Li − *Department of Chemical and Biomolecular Engineering and Beckman Institute for Advanced Science and Technology, University of Illinois at Urbana−Champaign, Urbana, Illinois 61801, United States; Joint Center for Energy Storage Research, Argonne National Laboratory, Lemont, Illinois 60439, United States*

Songsong Li − *Department of Materials Science and Engineering and Beckman Institute for Advanced Science and Technology, University of Illinois at Urbana−Champaign, Urbana, Illinois 61801, United States*

Yun Liu − *Department of Chemistry and Beckman Institute for Advanced Science and Technology, University of Illinois at Urbana−Champaign, Urbana, Illinois 61801, United States*

Nicholas E. Jackson − *Department of Chemistry and Beckman Institute for Advanced Science and Technology, University of Illinois at Urbana−Champaign, Urbana, Illinois 61801, United States;* orcid.org/0000-0002-1470-1903

Jeffrey S. Moore − *Department of Materials Science and Engineering, Department of Chemistry, and Beckman Institute for Advanced Science and Technology, University of Illinois at Urbana−Champaign, Urbana, Illinois 61801, United States; Joint Center for Energy Storage Research, Argonne National Laboratory, Lemont, Illinois 60439, United States*

Complete contact information is available at: https://pubs.acs.org/10.1021/jacs.1c12741

Author Contributions

#H.Y. and J.L. contributed equally to this work.

Notes

The authors declare no competing financial interest.

■ ACKNOWLEDGMENTS

This work was supported by the U.S. Department of Energy, Office of Basic Energy Sciences, Division of Materials Sciences and Engineering under Award No. DE-FG02-07ER46471 (H.Y. and J.S.M.), and by the Joint Center for Energy Storage Research (JCESR), an Energy Innovation Hub funded by the U.S. Department of Energy, Office of Science, Basic Energy Sciences through Argonne National Lab under Award No. DE-AC02-06CH11357 (J.L., S.L., and C.M.S.). We thank Toby Woods for X-ray diffraction analysis and Lingyang Zhu and Dean Olson for NMR assistance.

■ REFERENCES

(1) Coropceanu, V.; Cornil, J.; da Silva Filho, D. A.; Olivier, Y.; Silbey, R.; Brédas, J.-L. Charge Transport in Organic Semiconductors. *Chem. Rev.* **2007**, *107* (4), 926−952.

(2) Arnold, A. R.; Grodick, M. A.; Barton, J. K. DNA Charge Transport: From Chemical Principles to the Cell. *Cell Chem. Biol.* **2016**, *23* (1), 183−197.

(3) Brédas, J. L.; Calbert, J. P.; da Silva Filho, D. A.; Cornil, J. Organic Semiconductors: A Theoretical Characterization of the Basic Parameters Governing Charge Transport. *Proc. Natl. Acad. Sci. U. S. A.* **2002**, *99* (9), 5804−5809.

(4) Moon, H.; Zeis, R.; Borkent, E.-J.; Besnard, C.; Lovinger, A. J.; Siegrist, T.; Kloc, C.; Bao, Z. Synthesis, Crystal Structure, and Transistor Performance of Tetracene Derivatives. *J. Am. Chem. Soc.* **2004**, *126* (47), 15322−15323.

(5) Wang, C.; Dong, H.; Jiang, L.; Hu, W. Organic Semiconductor Crystals. *Chem. Soc. Rev.* **2018**, *47* (2), 422−500.

(6) Gray, H. B.; Winkler, J. R. Electron Flow through Proteins. *Chem. Phys. Lett.* **2009**, *483* (1), 1−9.

(7) Zheng, H.; Jiang, F.; He, R.; Yang, Y.; Shi, J.; Hong, W. Charge Transport through Peptides in Single-Molecule Electrical Measurements. *Chin. J. Chem.* **2019**, *37* (10), 1083−1096.

(8) Jeuken, L. J. C.; Jones, A. K.; Chapman, S. K.; Cecchini, G.; Armstrong, F. A. Electron-Transfer Mechanisms through Biological Redox Chains in Multicenter Enzymes. *J. Am. Chem. Soc.* **2002**, *124* (20), 5702−5713.
(9) Meyer, T. J.; Huynh, M. H. V.; Thorp, H. H. The Possible Role of Proton-Coupled Electron Transfer (PCET) in Water Oxidation by Photosystem II. *Angew. Chemie Int. Ed.* **2007**, *46* (28), 5284−5304.
(10) Yavin, E.; Boal, A. K.; Stemp, E. D. A.; Boon, E. M.; Livingston, A. L.; O'Shea, V. L.; David, S. S.; Barton, J. K. Protein−DNA Charge Transport: Redox Activation of a DNA Repair Protein by Guanine Radical. *Proc. Natl. Acad. Sci. U. S. A.* **2005**, *102* (10), 3546−3551.
(11) Seferos, D. S.; Trammell, S. A.; Bazan, G. C.; Kushmerick, J. G. Probing π-Coupling in Molecular Junctions. *Proc. Natl. Acad. Sci. U. S. A.* **2005**, *102* (25), 8821−8825.
(12) Schneebeli, S. T.; Kamenetska, M.; Cheng, Z.; Skouta, R.; Friesner, R. A.; Venkataraman, L.; Breslow, R. Single-Molecule Conductance through Multiple Π−π-Stacked Benzene Rings Determined with Direct Electrode-to-Benzene Ring Connections. *J. Am. Chem. Soc.* **2011**, *133* (7), 2136−2139.
(13) Wu, S.; González, M. T.; Huber, R.; Grunder, S.; Mayor, M.; Schönenberger, C.; Calame, M. Molecular Junctions Based on Aromatic Coupling. *Nat. Nanotechnol.* **2008**, *3* (9), 569−574.
(14) Martín, S.; Grace, I.; Bryce, M. R.; Wang, C.; Jitchati, R.; Batsanov, A. S.; Higgins, S. J.; Lambert, C. J.; Nichols, R. J. Identifying Diversity in Nanoscale Electrical Break Junctions. *J. Am. Chem. Soc.* **2010**, *132* (26), 9157−9164.
(15) Frisenda, R.; Janssen, V. A. E. C.; Grozema, F. C.; van der Zant, H. S. J.; Renaud, N. Mechanically Controlled Quantum Interference in Individual π-Stacked Dimers. *Nat. Chem.* **2016**, *8* (12), 1099−1104.
(16) Magyarkuti, A.; Adak, O.; Halbritter, A.; Venkataraman, L. Electronic and Mechanical Characteristics of Stacked Dimer Molecular Junctions. *Nanoscale* **2018**, *10* (7), 3362−3368.
(17) Fu, T.; Smith, S.; Camarasa-Gómez, M.; Yu, X.; Xue, J.; Nuckolls, C.; Evers, F.; Venkataraman, L.; Wei, S. Enhanced Coupling through π-Stacking in Imidazole-Based Molecular Junctions. *Chem. Sci.* **2019**, *10* (43), 9998−10002.
(18) Li, X.; Wu, Q.; Bai, J.; Hou, S.; Jiang, W.; Tang, C.; Song, H.; Huang, X.; Zheng, J.; Yang, Y.; Liu, J.; Hu, Y.; Shi, J.; Liu, Z.; Lambert, C. J.; Zhang, D.; Hong, W. Structure-Independent Conductance of Thiophene-Based Single-Stacking Junctions. *Angew. Chemie Int. Ed.* **2020**, *59* (8), 3280−3286.
(19) Tang, Y.; Zhou, Y.; Zhou, D.; Chen, Y.; Xiao, Z.; Shi, J.; Liu, J.; Hong, W. Electric Field-Induced Assembly in Single-Stacking Terphenyl Junctions. *J. Am. Chem. Soc.* **2020**, *142* (45), 19101−19109.
(20) Biedermann, F.; Scherman, O. A. Cucurbit[8]Uril Mediated Donor−Acceptor Ternary Complexes: A Model System for Studying Charge-Transfer Interactions. *J. Phys. Chem. B* **2012**, *116* (9), 2842−2849.
(21) Chen, H.; Fraser Stoddart, J. From Molecular to Supramolecular Electronics. *Nat. Rev. Mater.* **2021**, *6* (9), 804−828.
(22) Zhang, W.; Gan, S.; Vezzoli, A.; Davidson, R. J.; Milan, D. C.; Luzyanin, K. V.; Higgins, S. J.; Nichols, R. J.; Beeby, A.; Low, P. J.; Li, B.; Niu, L. Single-Molecule Conductance of Viologen-Cucurbit[8]-Uril Host-Guest Complexes. *ACS Nano* **2016**, *10* (5), 5212−5220.
(23) Wen, H.; Li, W.; Chen, J.; He, G.; Li, L.; Olson, M. A.; Sue, A. C. H.; Stoddart, J. F.; Guo, X. Complex Formation Dynamics in a Single-Molecule Electronic Device. *Sci. Adv.* **2016**, *2* (11). DOI: 10.1126/sciadv.1601113.
(24) Li, S.; Li, J.; Yu, H.; Pudar, S.; Li, B.; Rodríguez-López, J.; Moore, J. S.; Schroeder, C. M. Characterizing Intermolecular Interactions in Redox-Active Pyridinium-Based Molecular Junctions. *J. Electroanal. Chem.* **2020**, *875*, 114070.
(25) Barrow, S. J.; Kasera, S.; Rowland, M. J.; del Barrio, J.; Scherman, O. A. Cucurbituril-Based Molecular Recognition. *Chem. Rev.* **2015**, *115* (22), 12320−12406.
(26) Wu, G.; Szabó, I.; Rosta, E.; Scherman, O. A. Cucurbit[8]Uril-Mediated Pseudo[2,3]Rotaxanes. *Chem. Commun.* **2019**, *55* (88), 13227−13230.
(27) Yaliraki, S. N.; Ratner, M. A. Molecule-Interface Coupling Effects on Electronic Transport in Molecular Wires. *J. Chem. Phys.* **1998**, *109* (12), 5036−5043.
(28) Rochefort, A.; Martel, R.; Avouris, P. Electrical Switching in π-Resonant 1D Intermolecular Channels. *Nano Lett.* **2002**, *2* (8), 877−880.
(29) Zhang, Y.; Zhou, T.-Y.; Zhang, K.-D.; Dai, J.-L.; Zhu, Y.-Y.; Zhao, X. Encapsulation Enhanced Dimerization of a Series of 4-Aryl-N-Methylpyridinium Derivatives in Water: New Building Blocks for Self-Assembly in Aqueous Media. *Chem. − An Asian J.* **2014**, *9* (6), 1530−1534.
(30) Zhang, K.-D.; Tian, J.; Hanifi, D.; Zhang, Y.; Sue, A. C.-H.; Zhou, T.-Y.; Zhang, L.; Zhao, X.; Liu, Y.; Li, Z.-T. Toward a Single-Layer Two-Dimensional Honeycomb Supramolecular Organic Framework in Water. *J. Am. Chem. Soc.* **2013**, *135* (47), 17913−17918.
(31) Lebègue, E.; Agullo, J.; Bélanger, D. Electrochemical Behavior of Pyridinium and N-Methyl Pyridinium Cations in Aqueous Electrolytes for CO2 Reduction. *ChemSusChem* **2018**, *11* (1), 219−228.
(32) Ohisa, S.; Pu, Y.-J.; Kido, J. Poly(Pyridinium Iodide Ionic Liquid)-Based Electron Injection Layers for Solution-Processed Organic Light-Emitting Devices. *J. Mater. Chem. C* **2016**, *4* (28), 6713−6719.
(33) Montoto, E. C.; Nagarjuna, G.; Hui, J.; Burgess, M.; Sekerak, N. M.; Hernández-Burgos, K.; Wei, T.-S.; Kneer, M.; Grolman, J.; Cheng, K. J.; Lewis, J. A.; Moore, J. S.; Rodríguez-López, J. Redox Active Colloids as Discrete Energy Storage Carriers. *J. Am. Chem. Soc.* **2016**, *138* (40), 13230−13237.
(34) Cheng, Y. C.; Silbey, R. J.; Da Silva Filho, D. A.; Calbert, J. P.; Cornil, J.; Brédas, J. L. Three-Dimensional Band Structure and Bandlike Mobility in Oligoacene Single Crystals: A Theoretical Investigation. *J. Chem. Phys.* **2003**, *118* (8), 3764−3774.
(35) Vura-Weis, J.; Ratner, M. A.; Wasielewski, M. R. Geometry and Electronic Coupling in Perylenediimide Stacks: Mapping Structure - Charge Transport Relationships. *J. Am. Chem. Soc.* **2010**, *132* (6), 1738−1739.
(36) Capozzi, B.; Dell, E. J.; Berkelbach, T. C.; Reichman, D. R.; Venkataraman, L.; Campos, L. M. Length-Dependent Conductance of Oligothiophenes. *J. Am. Chem. Soc.* **2014**, *136* (29), 10486−10492.
(37) Li, B.; Yu, H.; Montoto, E. C.; Liu, Y.; Li, S.; Schwieter, K.; Rodríguez-López, J.; Moore, J. S.; Schroeder, C. M. Intrachain Charge Transport through Conjugated Donor−Acceptor Oligomers. *ACS Appl. Electron. Mater.* **2019**, *1* (1), 7−12.
(38) Su, T. A.; Neupane, M.; Steigerwald, M. L.; Venkataraman, L.; Nuckolls, C. Chemical Principles of Single-Molecule Electronics. *Nat. Rev. Mater.* **2016**, *1*, 16002.
(39) Senler, S.; Cui, L.; Broomes, A. M.; Smith, E. L.; Wilson, J. N.; Kaifer, A. E. New Guests for the Cucurbit[8]Uril Host. Formation of G2H Ternary Complexes. *J. Phys. Org. Chem.* **2012**, *25* (7), 592−596.
(40) Schoder, S.; Schalley, C. A. Orthogonal Switching of Self-Sorting Processes in a Stimuli-Responsive Library of Cucurbit[8]Uril Complexes. *Chem. Commun.* **2017**, *53* (69), 9546−9549.
(41) Martinez, C. R.; Iverson, B. L. Rethinking the Term "Pi-Stacking. *Chem. Sci.* **2012**, *3* (7), 2191−2201.
(42) Zhang, Z.-J.; Zhang, Y.-M.; Liu, Y. Controlled Molecular Self-Assembly Behaviors between Cucurbituril and Bispyridinium Derivatives. *J. Org. Chem.* **2011**, *76* (11), 4682−4685.
(43) Lagona, J.; Mukhopadhyay, P.; Chakrabarti, S.; Isaacs, L. The Cucurbit[n]Uril Family. *Angew. Chemie Int. Ed.* **2005**, *44* (31), 4844−4870.
(44) Wu, G.; Bae, Y. J.; Olesińska, M.; Antón-García, D.; Szabó, I.; Rosta, E.; Wasielewski, M. R.; Scherman, O. A. Controlling the Structure and Photophysics of Fluorophore Dimers Using Multiple Cucurbit[8]Uril Clampings. *Chem. Sci.* **2020**, *11* (3), 812−825.

(45) Yu, H.; Li, S.; Schwieter, K. E.; Liu, Y.; Sun, B.; Moore, J. S.; Schroeder, C. M. Charge Transport in Sequence-Defined Conjugated Oligomers. *J. Am. Chem. Soc.* **2020**, *142* (10), 4852−4861.
(46) Li, S.; Yu, H.; Schwieter, K.; Chen, K.; Li, B.; Liu, Y.; Moore, J. S.; Schroeder, C. M. Charge Transport and Quantum Interference Effects in Oxazole-Terminated Conjugated Oligomers. *J. Am. Chem. Soc.* **2019**, *141* (40), 16079−16084.
(47) Chen, H.; Brasiliense, V.; Mo, J.; Zhang, L.; Jiao, Y.; Chen, Z.; Jones, L. O.; He, G.; Guo, Q.-H.; Chen, X.-Y.; Song, B.; Schatz, G. C.; Stoddart, J. F. Single-Molecule Charge Transport through Positively Charged Electrostatic Anchors. *J. Am. Chem. Soc.* **2021**, *143* (7), 2886−2895.
(48) Tang, C.; Zheng, J.; Ye, Y.; Liu, J.; Chen, L.; Yan, Z.; Chen, Z.; Chen, L.; Huang, X.; Bai, J.; Chen, Z.; Shi, J.; Xia, H.; Hong, W. Electric-Field-Induced Connectivity Switching in Single-Molecule Junctions. *iScience* **2020**, *23* (1), 100770.
(49) Walsh-Korb, Z.; Yu, Y.; Janeček, E. R.; Lan, Y.; Del Barrio, J.; Williams, P. E.; Zhang, X.; Scherman, O. A. Single-Molecule Force Spectroscopy Quantification of Adhesive Forces in Cucurbit[8]Uril Host-Guest Ternary Complexes. *Langmuir* **2017**, *33* (6), 1343−1350.
(50) Leary, E.; La Rosa, A.; González, M. T.; Rubio-Bollinger, G.; Agraït, N.; Martín, N. Incorporating Single Molecules into Electrical Circuits. the Role of the Chemical Anchoring Group. *Chem. Soc. Rev.* **2015**, *44* (4), 920−942.
(51) Venkataraman, L.; Klare, J. E.; Nuckolls, C.; Hybertsen, M. S.; Steigerwald, M. L. Dependence of Single-Molecule Junction Conductance on Molecular Conformation. *Nature* **2006**, *442* (7105), 904−907.
(52) Kamenetska, M.; Koentopp, M.; Whalley, A. C.; Park, Y. S.; Steigerwald, M. L.; Nuckolls, C.; Hybertsen, M. S.; Venkataraman, L. Formation and Evolution of Single-Molecule Junctions. *Phys. Rev. Lett.* **2009**, *102* (12), 126803.
(53) Kim, N. T.; Li, H.; Venkataraman, L.; Leighton, J. L. High-Conductance Pathways in Ring-Strained Disilanes by Way of Direct σ-Si−Si to Au Coordination. *J. Am. Chem. Soc.* **2016**, *138* (36), 11505−11508.
(54) Adak, O.; Rosenthal, E.; Meisner, J.; Andrade, E. F.; Pasupathy, A. N.; Nuckolls, C.; Hybertsen, M. S.; Venkataraman, L. Flicker Noise as a Probe of Electronic Interaction at Metal-Single Molecule Interfaces. *Nano Lett.* **2015**, *15* (6), 4143−4149.
(55) Xin, N.; Guan, J.; Zhou, C.; Chen, X.; Gu, C.; Li, Y.; Ratner, M. A.; Nitzan, A.; Stoddart, J. F.; Guo, X. Concepts in the Design and Engineering of Single-Molecule Electronic Devices. *Nat. Rev. Phys.* **2019**, *1* (3), 211−230.
(56) Kaliginedi, V.; Rudnev, A. V.; Moreno-García, P.; Baghernejad, M.; Huang, C.; Hong, W.; Wandlowski, T. Promising Anchoring Groups for Single-Molecule Conductance Measurements. *Phys. Chem. Chem. Phys.* **2014**, *16* (43), 23529−23539.
(57) Obersteiner, V.; Egger, D. A.; Zojer, E. Impact of Anchoring Groups on Ballistic Transport: Single Molecule vs Monolayer Junctions. *J. Phys. Chem. C* **2015**, *119* (36), 21198−21208.
(58) Martín, S.; Manrique, D. Z.; García-Suárez, V. M.; Haiss, W.; Higgins, S. J.; Lambert, C. J.; Nichols, R. J. Adverse Effects of Asymmetric Contacts on Single Molecule Conductances of HS-(CH2)NCOOH in Nanoelectrical Junctions. *Nanotechnology* **2009**, *20* (12), 125203.
(59) Wu, G.; Olesińska, M.; Wu, Y.; Matak-Vinkovic, D.; Scherman, O. A. Mining 2:2 Complexes from 1:1 Stoichiometry: Formation of Cucurbit[8]Uril−Diarylviologen Quaternary Complexes Favored by Electron-Donating Substituents. *J. Am. Chem. Soc.* **2017**, *139* (8), 3202−3208.
(60) Roman, T.; Groß, A. Periodic Density-Functional Calculations on Work-Function Change Induced by Adsorption of Halogens on Cu(111). *Phys. Rev. Lett.* **2013**, *110* (15), 1−4.
(61) Roman, T.; Gossenberger, F.; Forster-Tonigold, K.; Groß, A. Halide Adsorption on Close-Packed Metal Electrodes. *Phys. Chem. Chem. Phys.* **2014**, *16* (27), 13630−13634.
(62) Shatla, A. S.; Abd-El-Latif, A. A.; Ayata, S.; Demir, D.; Baltruschat, H. Iodide Adsorption at Au(111) Electrode in Non-Aqueous Electrolyte: AC-Voltammetry and EIS Studies. *Electrochim. Acta* **2020**, *334*, 135556.
(63) Marenich, A. V.; Cramer, C. J.; Truhlar, D. G. Universal Solvation Model Based on Solute Electron Density and on a Continuum Model of the Solvent Defined by the Bulk Dielectric Constant and Atomic Surface Tensions. *J. Phys. Chem. B* **2009**, *113* (18), 6378−6396.
(64) Frisch, M. J.; Trucks, G. W.; Schlegel, H. B.; Scuseria, G. E.; Robb, M. a.; Cheeseman, J. R.; Scalmani, G.; Barone, V.; Petersson, G. a.; Nakatsuji, H.; Li, X.; Caricato, M.; Marenich, a. V.; Bloino, J.; Janesko, B. G.; Gomperts, R.; Mennucci, B.; Hratchian, H. P.; Ortiz, J. V.; Izmaylov, a. F.; Sonnenberg, J. L.; Williams; Ding, F.; Lipparini, F.; Egidi, F.; Goings, J.; Peng, B.; Petrone, A.; Henderson, T.; Ranasinghe, D.; Zakrzewski, V. G.; Gao, J.; Rega, N.; Zheng, G.; Liang, W.; Hada, M.; Ehara, M.; Toyota, K.; Fukuda, R.; Hasegawa, J.; Ishida, M.; Nakajima, T.; Honda, Y.; Kitao, O.; Nakai, H.; Vreven, T.; Throssell, K.; Montgomery, J. A., Jr.; Peralta, J. E.; Ogliaro, F.; Bearpark, M. J.; Heyd, J. J.; Brothers, E. N.; Kudin, K. N.; Staroverov, V. N.; Keith, T. a.; Kobayashi, R.; Normand, J.; Raghavachari, K.; Rendell, a. P.; Burant, J. C.; Iyengar, S. S.; Tomasi, J.; Cossi, M.; Millam, J. M.; Klene, M.; Adamo, C.; Cammi, R.; Ochterski, J. W.; Martin, R. L.; Morokuma, K.; Farkas, O.; Foresman, J. B.; Fox, D. J. *Gaussian 16*, Revision C.01; Gaussian, Inc.: Wallingford, CT, 2016.
(65) Chai, J.-D.; Head-Gordon, M. Systematic Optimization of Long-Range Corrected Hybrid Density Functionals. *J. Chem. Phys.* **2008**, *128* (8), 84106.
(66) Chai, J.-D.; Head-Gordon, M. Long-Range Corrected Hybrid Density Functionals with Damped Atom−Atom Dispersion Corrections. *Phys. Chem. Chem. Phys.* **2008**, *10* (44), 6615−6620.
(67) Kondo, H.; Nara, J.; Kino, H.; Ohno, T. Dependence of the Conduction of a Single Biphenyl Dithiol Molecule on the Dihedral Angle between the Phenyl Rings and Its Application to a Nanorectifier. *J. Chem. Phys.* **2008**, *128* (6), 64701.
(68) Vonlanthen, D.; Mishchenko, A.; Elbing, M.; Neuburger, M.; Wandlowski, T.; Mayor, M. Chemically Controlled Conductivity: Torsion-Angle Dependence in a Single-Molecule Biphenyldithiol Junction. *Angew. Chemie Int. Ed.* **2009**, *48* (47), 8886−8890.
(69) *Synopsys QuantumATK Home Page.* https://www.synopsys.com/silicon/quantumatk.html (accessed Feb 01, 2022).
(70) Smidstrup, S.; Markussen, T.; Vancraeyveld, P.; Wellendorff, J.; Schneider, J.; Gunst, T.; Verstichel, B.; Stradi, D.; Khomyakov, P. A.; Vej-Hansen, U. G.; others. QuantumATK: An Integrated Platform of Electronic and Atomic-Scale Modelling Tools. *J. Phys.: Condens. Matter* **2020**, *32*, 15901.
(71) Cai, Z.; Lo, W.-Y.; Zheng, T.; Li, L.; Zhang, N.; Hu, Y.; Yu, L. Exceptional Single-Molecule Transport Properties of Ladder-Type Heteroacene Molecular Wires. *J. Am. Chem. Soc.* **2016**, *138* (33), 10630−10635.
(72) Wang, K.; Vezzoli, A.; Grace, I. M.; McLaughlin, M.; Nichols, R. J.; Xu, B.; Lambert, C. J.; Higgins, S. J. Charge Transfer Complexation Boosts Molecular Conductance through Fermi Level Pinning. *Chem. Sci.* **2019**, *10* (8), 2396−2403.
(73) Vezzoli, A.; Grace, I.; Brooke, C.; Wang, K.; Lambert, C. J.; Xu, B.; Nichols, R. J.; Higgins, S. J. Gating of Single Molecule Junction Conductance by Charge Transfer Complex Formation. *Nanoscale* **2015**, *7* (45), 18949−18955.
(74) Valeev, E. F.; Coropceanu, V.; da Silva Filho, D. A.; Salman, S.; Brédas, J.-L. Effect of Electronic Polarization on Charge-Transport Parameters in Molecular Organic Semiconductors. *J. Am. Chem. Soc.* **2006**, *128* (30), 9882−9886.
(75) Fazzi, D.; Caironi, M.; Castiglioni, C. Quantum-Chemical Insights into the Prediction of Charge Transport Parameters for a Naphthalenetetracarboxydiimide-Based Copolymer with Enhanced Electron Mobility. *J. Am. Chem. Soc.* **2011**, *133* (47), 19056−19059.
(76) Troisi, A. Charge Transport in High Mobility Molecular Semiconductors: Classical Models and New Theories. *Chem. Soc. Rev.* **2011**, *40* (5), 2347−2358.
(77) Liu, Y.; Ornago, L.; Carlotti, M.; Ai, Y.; El Abbassi, M.; Soni, S.; Asyuda, A.; Zharnikov, M.; van der Zant, H. S. J.; Chiechi, R. C.

Intermolecular Effects on Tunneling through Acenes in Large-Area and Single-Molecule Junctions. *J. Phys. Chem. C* **2020**, *124* (41), 22776−22783.
(78) Li, J.; Shen, P.; Zhen, S.; Tang, C.; Ye, Y.; Zhou, D.; Hong, W.; Zhao, Z.; Tang, B. Z. Mechanical Single-Molecule Potentiometers with Large Switching Factors from Ortho-Pentaphenylene Foldamers. *Nat. Commun.* **2021**, *12* (1), 167.
(79) Fujii, S.; Tada, T.; Komoto, Y.; Osuga, T.; Murase, T.; Fujita, M.; Kiguchi, M. Rectifying Electron-Transport Properties through Stacks of Aromatic Molecules Inserted into a Self-Assembled Cage. *J. Am. Chem. Soc.* **2015**, *137* (18), 5939−5947.
(80) Jeon, W. S.; Kim, H.-J.; Lee, C.; Kim, K. Control of the Stoichiometry in Host−Guest Complexation by Redox Chemistry of Guests: Inclusion of Methylviologen in Cucurbit[8]Uril. *Chem. Commun.* **2002**, *17*, 1828−1829.
(81) Hwang, I.; Ziganshina, A. Y.; Ko, Y. H.; Yun, G.; Kim, K. A New Three-Way Supramolecular Switch Based on Redox-Controlled Interconversion of Hetero- and Homo-Guest-Pair Inclusion inside a Host Molecule. *Chem. Commun.* **2009**, *4*, 416−418.
(82) Sonzini, S.; Ryan, S. T. J.; Scherman, O. A. Supramolecular Dimerisation of Middle-Chain Phe Pentapeptides via CB[8] Host−Guest Homoternary Complex Formation. *Chem. Commun.* **2013**, *49* (78), 8779−8781.
(83) Heitmann, L. M.; Taylor, A. B.; Hart, P. J.; Urbach, A. R. Sequence-Specific Recognition and Cooperative Dimerization of N-Terminal Aromatic Peptides in Aqueous Solution by a Synthetic Host. *J. Am. Chem. Soc.* **2006**, *128* (38), 12574−12581.
(84) Nagarjuna, G.; Hui, J.; Cheng, K. J.; Lichtenstein, T.; Shen, M.; Moore, J. S.; Rodríguez-López, J. Impact of Redox-Active Polymer Molecular Weight on the Electrochemical Properties and Transport across Porous Separators in Nonaqueous Solvents. *J. Am. Chem. Soc.* **2014**, *136* (46), 16309−16316.
(85) Pazos, E.; Novo, P.; Peinador, C.; Kaifer, A. E.; García, M. D. Cucurbit[8]Uril (CB[8])-Based Supramolecular Switches. *Angew. Chemie - Int. Ed.* **2019**, *58* (2), 403−416.

https://doi.org/10.1021/jacs.1c12741
J. Am. Chem. Soc. 2022, 144, 3162−3173